ACS APPLIED MATERIALS & INTERFACES

Research Article

www.acsami.org

Electrolyte Effect on the Electrochemical Performance of Mild Aqueous Zinc-Electrolytic Manganese Dioxide Batteries

Huilin Pan,* Jacob F. Ellis, Xiaolin Li, Zimin Nie, Hee Jung Chang, and David Reed

Energy & Environment Directorate, Pacific Northwest National Laboratory, Richland, Washington 99354, United States

Supporting Information

ABSTRACT: Recently, mild aqueous rechargeable Zn-MnO_2 batteries have attracted increasing interest for energy storage due to the low cost of Zn and Mn resources, high safety, and environmental benignity. Extensive types of MnO_2 have been proposed as the cathodes in the literature, but the different reported performance and lack of a thorough understanding of reactions in MnO_2 cathodes greatly hinder the practical applications of mild aqueous Zn-MnO_2 batteries. Here, we revealed the correlation between the reaction mechanisms and the used electrolytes for the mild aqueous zinc-electrolytic manganese dioxide (EMD) batteries. In optimal $Zn(TFSI)_2$-based electrolyte, the EMD cathode exhibits a mixed diffusion-controlled conversion reaction between EMD and H^+ and diffusion-free "pseudocapacitance"-like reactions. This mechanism enables excellent cycling stability of an EMD cathode over 5000 cycles with a capacity retention of 94.6%. This study provides a useful insight into developing reversible MnO_2 cathodes through rational control of reaction mechanisms for high performance mild aqueous Zn-MnO_2 batteries.

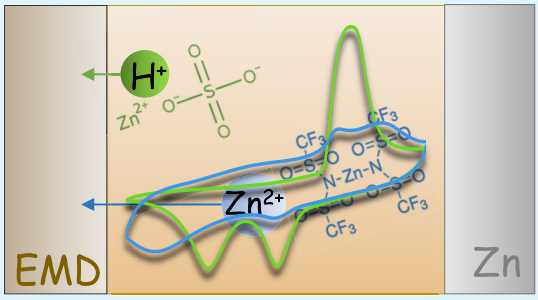

KEYWORDS: *mild aqueous Zn-MnO_2 batteries, electrolytic manganese dioxide, reaction mechanism, mixed charge storage, electrolyte effect*

INTRODUCTION

Aqueous Zn-MnO_2 batteries, first recognized in the 1950s in primary alkaline batteries,[1,2] have recently regained increasing interest for the applications of the large-scale grid energy storage because of low cost, high energy density, and high environmental benignity.[3−6] The extensive effort of converting primary alkaline Zn-MnO_2 batteries to be rechargeable goes back to the 1970s through a shallow discharge protocol and optimized MnO_2 cathodes, etc.[6−9] The cycling stability of rechargeable alkaline Zn-MnO_2 batteries is still challenging for their practical applications due to Zn dendrite formation and passivation and the crystal structure degradation of the MnO_2 cathode during the deep discharge process in alkaline electrolytes.[10]

Recently, mild aqueous electrolytes have attracted increasing interest for rechargeable Zn-MnO_2 batteries, which present attractive advantages, such as no limitation of the depth of discharge (DOD) and highly reversible Zn anode reaction.[3,11−13] MnO_2 with different morphologies and crystal structures, for example, various nanostructured α-,[3,14,15] β-,[4] γ-,[16] δ-,[17] and akhtenskite[18] phases, have been proposed as cathode materials for mild aqueous rechargeable Zn-MnO_2 batteries. Nevertheless, the synthesis method of MnO_2 cathodes and their performance vary remarkably in the literature. Furthermore, the reaction mechanisms for polymorph MnO_2 remain controversial and complex, for example, Zn^{2+} ion intercalation in different phases of MnO_2 forming spinel $ZnMn_2O_4$,[14] buserite Zn_xMnO_2,[15] tunnel-type γ-Zn_xMnO_2 and layered-type L-Zn_yMnO_2, etc.,[16] H^+ ion reaction with α-MnO_2 forming MnOOH,[3] and coinsertion of Zn^{2+} and H^+ ions.[5,18] We recently found that the charge storage mechanisms and transport properties in nanoflake δ-MnO_2 could be manipulated through the used electrolyte, through which a joint charge storage reaction was identified in appropriate electrolyte, enabling a highly reversible δ-MnO_2 cathode.[19] Among various MnO_2 materials, electrolytic manganese dioxide (EMD) has been used as a cathode material in commercial alkaline batteries, which shows significant advantages for practical applications such as low synthesis cost and large-scale commercial availability.[20,21] It will be worth investigating the electrolyte effect on the electrochemical performance of EMD as a cathode for mild aqueous Zn-MnO_2 batteries from a practical perspective.

In this work, we demonstrate the EMD material as a promising cathode material for the application of long-life and high-rate aqueous rechargeable Zn-MnO_2 batteries. The effective redox reactions in EMD cathodes were systematically investigated in different electrolytes, showing a strong correlation with the employed electrolytes. A mixed diffusion-controlled conversion reaction between EMD and H^+ and diffusion-free "pseudocapacitance"-like reactions were revealed. With appropriate $Zn(TFSI)_2$-based electrolyte, the EMD cathode shows high-rate and ultrastable cycling over 5000 cycles with no visible degradation based on the mixed

Received: June 3, 2019
Accepted: September 16, 2019
Published: September 16, 2019

ACS Publications © XXXX American Chemical Society

DOI: 10.1021/acsami.9b09252
ACS Appl. Mater. Interfaces XXXX, XXX, XXX−XXX

charge storage mechanism. The electrolyte-dependent mixed charge storage reactions in the EMD cathode in this work are similar to the joint charge storage in a layered δ-MnO_2 cathode in a previous report.[19] Interestingly, the electrolyte-dependent mixed charge storage seems not limited to a special crystal phase or morphology of MnO_2 material. This study provides useful guidance to develop a highly reversible MnO_2 cathode through the control of the reaction mechanisms for high performance mild aqueous Zn-MnO_2 batteries.

■ EXPERIMENTAL PROCEDURES

EMD material was obtained from TRONOX LLC. The $ZnSO_4 \cdot 7H_2O$ (99%, Sigma-Aldrich), $MnSO_4 \cdot H_2O$ (99%, Sigma-Aldrich), Zn-$(TFSI)_2$ (99.5%, Solvionic), and $Mn(TFSI)_2$ (99.5%, Solvionic) were used as the electrolyte salts and additives. Zinc salt electrolytes (1 M and 3 M) were prepared by dissolving 1 and 3 mol zinc slats into 1 L of deionized water (DI water), respectively. Electrolytes with 0.1 M manganese salt additive were prepared by adding 0.1 mol of manganese salt into electrolyte containing 1 L of DI water. Zinc foil (99.9%, Alfa Arsar) was punched into a 9/16" disk and used as the anode. X-ray diffraction (XRD) for cycled EMD electrodes before and after DI water rinsing was conducted on a Rigaku Miniflex II diffractometer (Cu Kα radiation, λ= 1.5406 Å). Scanning electron microscopy (SEM) images were performed using a helium ion microscope.

EMD electrodes were prepared by mixing EMD, acetylene black, and PVDF binder at a weight ratio of 60:30:10 in NMP solvent and casting the mixture onto carbon paper. The EMD electrodes were dried at 80 °C under vacuum for 10 h before assembling cells. The EMD mass loading in electrode is ~1 mg cm^{-2}. 2032 coin cells were prepared using an EMD electrode (1/2" in diameter) as the cathode, Zn foil (9/16" in diameter) as the counter electrode, and a glass fiber disk (3/4" in diameter) as the separator. Symmetrical EMD||EMD and Zn||Zn cells were assembled with fresh EMD and Zn anode electrodes, respectively. The charge−discharge was performed on a LANHER battery tester (Wuhan) during 1−1.8 V. Cyclic voltammetry (CV) measurements were carried out for Zn-EMD coin cells using CHI660E in a scanning rate of 0.1−10 mV s^{-1}. Electrochemical impedance spectra (EIS) measurement was conducted on Bio-Logic Instruments (VSP) for EMD||EMD, Zn||Zn, and EMD||Zn cells.

■ RESULTS AND DISCUSSION

Figure 1a shows the XRD pattern of EMD material with a defect crystal phase that can be adequately described as γ-MnO_2 or ε-MnO_2.[22] The SEM images of EMD material indicate a particle size of 5−20 μm which is built up with nanoparticles (Figure 1b and 1c). The hierarchical structure of EMD is ascribed to the electrodeposition process of the material,[23] which could be beneficial to the transport of electrons and ions inside the EMD particles.

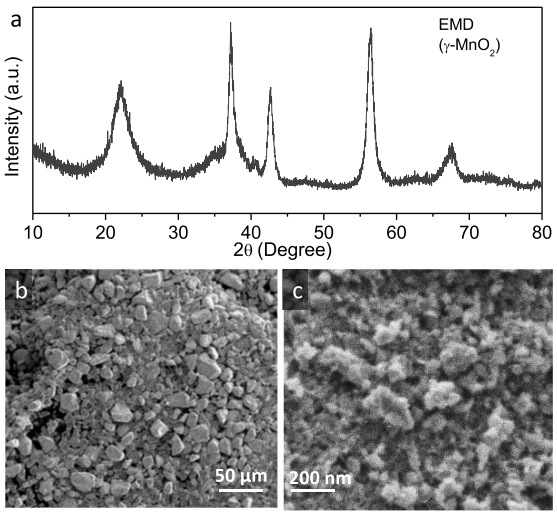

Figure 1. (a) XRD pattern and (b), (c) SEM images of EMD powder.

The electrochemical and structural stability of the EMD cathode strongly associates with the redox reactions occurring in the electrode and electrode/electrolyte interface, in which the electrolyte components play a key role in determining the practical reactions. The impact of different electrolytes on the electrochemical performance of EMD was investigated in Figure 2. The cyclic voltammetry (CV) measurements for EMD cathodes (second cycle) exhibit remarkably different curves in electrolytes with different salts (Figure 2a). In 1 M $ZnSO_4$ electrolyte, two obvious reduction peaks located at 1.40 and 1.219 V and one main oxidation peak at 1.59 V were observed for the redox reactions in the EMD cathode. While in 1 M $Zn(TFSI)_2$ electrolyte, the EMD cathode exhibits a compressed CV shape with wider anodic peaks at 1.395 and 1.071 V and a cathodic bump starting from ~1.3 V and followed by a bimodal peak around 1.6 V. In agreement with the CV curves, the EMD cathode shows two plateaus during discharge and one plateau during charge in 1 M $ZnSO_4$ electrolyte (Figure 2b). In contrary, the charge−discharge plateaus of EMD became less obvious in 1 M $Zn(TFSI)_2$ electrolyte, showing a slope-like behavior in the second cycle (Figure 2b). (Note that the Zn-EMD cells show a difference in the discharge curves during the first and second cycle as reported in a previous report (Figure S1).[3]) This indicates

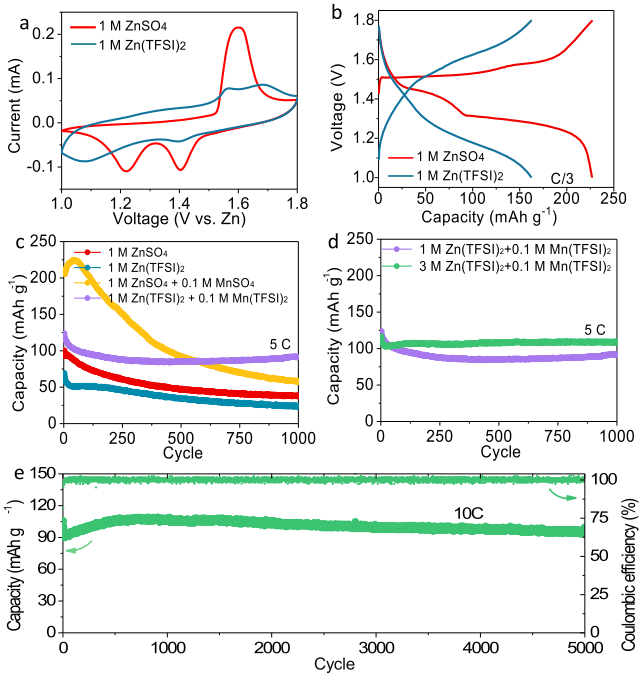

Figure 2. (a) Cyclic voltammetry of Zn-EMD batteries in 1 M $ZnSO_4$ and 1 M $Zn(TFSI)_2$ electrolytes (0.1 mV s^{-1}, second cycle). (b) Charge−discharge profiles for Zn-EMD cells in 1 M $ZnSO_4$ and 1 M $Zn(TFSI)_2$ electrolyte, respectively, at C/3 (second cycle). (c), (d) Cycling performance of EMD cathodes in different electrolytes at 5 C after the first 3 cycles at a lower rate of C/3 (Figure S4). (e) Long-term cycling performance of the Zn-EMD cell at 10 C in 3 M $Zn(TFSI)_2$ + 0.1 M $Mn(TFSI)_2$ electrolyte.

DOI: 10.1021/acsami.9b09252
ACS Appl. Mater. Interfaces XXXX, XXX, XXX−XXX

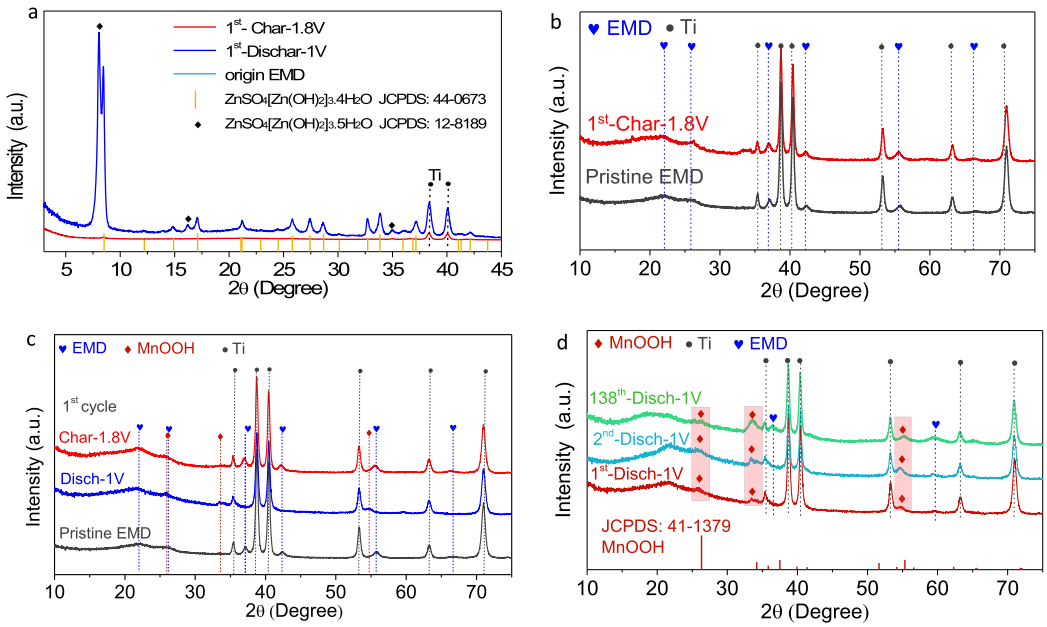

Figure 3. XRD patterns of EMD electrodes in (a), (b) 1 M $ZnSO_4$ electrolyte and (c), (d) 3 M $Zn(TFSI)_2$ electrolyte during charge and discharge at C/3. Ti foil was used as a substrate for the EMD electrode for the XRD analysis. Circle, Ti; diamond, MnOOH; heart, EMD.

different redox reactions in EMD cathodes in different electrolytes, which is similar to a previous report in the δ-MnO_2 cathode.[19]

In addition, the electrochemical cycling performance of EMD cathodes in different electrolytes was investigated in Figure 2c. EMD cathodes show limited capacity of 100.3 and 69.3 mAh g^{-1} at 5 C in 1 M $ZnSO_4$ (red curve) and 1 M $Zn(TFSI)_2$ (blue curve), respectively, in the first cycle under 5 C rate. The capacities fade in initial cycles in both electrolytes due to the Mn^{2+} dissolution from the EMD cathode (Figure S2), which is similar to the capacity degradation in other types of MnO_2 cathodes.[3,24,25] Interestingly, the capacity decay due to Mn^{2+} dissolution in 1 M $ZnSO_4$ electrolyte (red curves) is much faster than that in 1 M $Zn(TFSI)_2$ electrolyte (blue curve). The total mass loss from the EMD cathode after 50 cycles in 1 M $ZnSO_4$ electrolyte is about 6 times larger than that in 1 M $Zn(TFSI)_2$ electrolyte as shown in Figure S2. This indicates that the specification of zinc salt in aqueous electrolyte could strongly affect the stability of reactions in EMD cathodes.

According to a previous report, an optimal amount of preaddition of Mn^{2+} ions in electrolyte would facilitate the MnO_2 cathode, reaching stability by providing an equilibrium between Mn^{2+} dissolution and reprecipitation.[3] 0.1 M $MnSO_4$ and 0.1 M $Mn(TFSI)_2$ were added into 1 M $ZnSO_4$ and 1 M $Zn(TFSI)_2$ electrolytes, respectively, in this work. The capacity of EMD significantly increased to 212 mAh g^{-1} (yellow curve) and 123 mAh g^{-1} (purple curve) after Mn^{2+} addition, respectively (Figure 2c). The EMD cathode exhibited remarkable improvement to the cycling performance in 1 M $Zn(TFSI)_2$ + 0.1 M $Mn(TFSI)_2$ electrolyte, whereas capacity fading of the EMD cathode in 1 M $ZnSO_4$ + 0.1 M $MnSO_4$ electrolyte was not improved obviously. The different improvement in the cycling stability for EMD cathodes after preaddition of Mn^{2+} in electrolytes could be related to varying kinetics of Mn^{2+} dissolution/precipitation in different conditions, such as the electrode structure and surface properties of the MnO_2 cathode and concentrations of salts in different electrolytes.[26−29]

Based on the better cycling stability of EMD in $Zn(TFSI)_2$-based electrolyte, a different concentration of $Zn(TFSI)_2$ salts was further investigated in Figure 2d. It was found that higher concentration of $Zn(TFSI)_2$ salt (green curve) can further enhance the cycling stability and capacity of EMD compared with those in electrolyte of 1 M $Zn(TFSI)_2$ + 0.1 M $Mn(TFSI)_2$ over 1000 cycles at 5 C. This could be ascribed to the further stabilized EMD cathode against Mn^{2+} dissolution by reducing the activity of water-based electrolyte under higher salt concentration.[30] The charge−discharge curves of the EMD cathode retain overlapping during cycling (Figure S3). Furthermore, the EMD cathode also demonstrates high rate performance with a reversible capacity of 105 mAh g^{-1} at 10 C, Coulombic efficiency of ∼100%, and excellent cycling stability with a capacity retention of 94.6% over 5000 cycles (Figure 2e).

To understand the reactions for EMD cathodes in different electrolytes, the structural evolution of EMD along cycling was investigated in Figure 3. Electrolytes without Mn^{2+} addition were used for EMD electrodes to simplify the XRD analysis by avoiding the interference from oxidation of the Mn^{2+} additive in electrolytes. The XRD patterns of EMD electrodes in 1 M $ZnSO_4$ electrolyte for the first cycle were shown in Figure 3a and 3b after rinsing with DI water. Note that DI water rinsing does not change the XRD patterns of EMD electrodes as shown in Figure S5. Newly formed discharged products of $ZnSO_4[Zn(OH)_2]_3{\cdot}nH_2O$ (n = 3, 4, and/or 5) were clearly observed in an EMD electrode at 1 V. This is consistent with the previous report on the reversible formation of $ZnSO_4[Zn(OH)_2]_3{\cdot}nH_2O$ on α-MnO_2 and δ-MnO_2 cathodes in $ZnSO_4$-based electrolyte.[3,24] The reversible formation of $ZnSO_4[Zn(OH)_2]_3{\cdot}nH_2O$ is accompanied by the reversible redox reaction between the H^+ ion and EMD cathode to form MnOOH during charge and discharge through the following reactions:

DOI: 10.1021/acsami.9b09252
ACS Appl. Mater. Interfaces XXXX, XXX, XXX−XXX

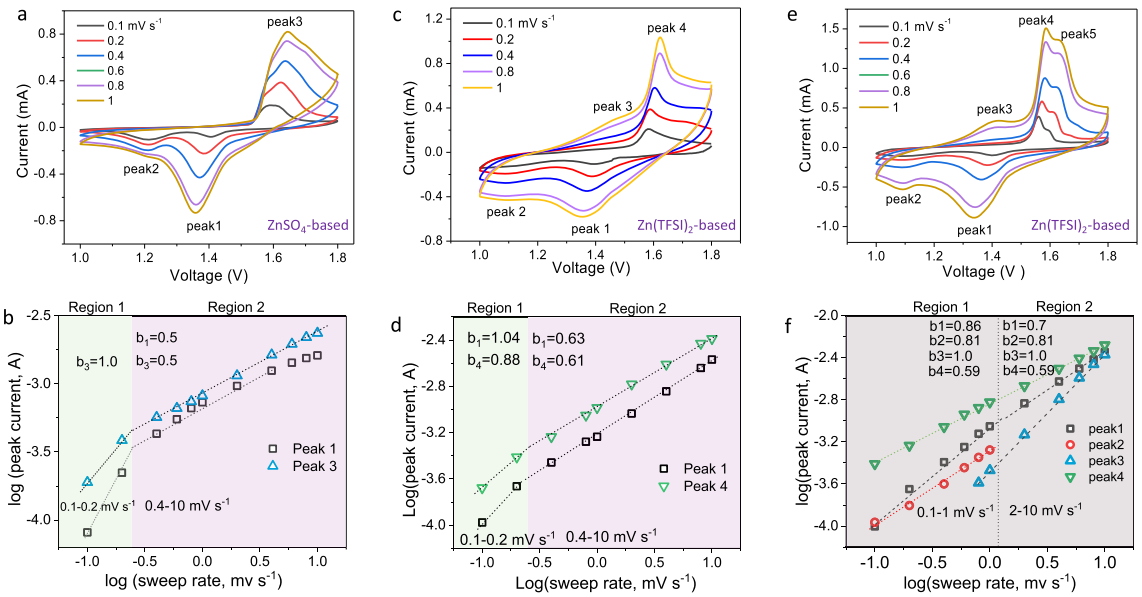

Figure 4. CV curves of Zn-EMD batteries at different scan rate in electrolytes of (a) 1 M $ZnSO_4$, (c) 3 M $Zn(TFSI)_2$, and (e) 3 M $Zn(TFSI)_2$ + 0.1 M $Mn(TFSI)_2$, respectively. The *b*-value of each peak is fitted according to $i = av^b$ (*i* is current; *a*, *b* are varying values; *v* is scanning rate) for an electrolyte of (b) 1 M $ZnSO_4$, (d) 3 M $Zn(TFSI)_2$, and (f) 3 M $Zn(TFSI)_2$ + 0.1 M $Mn(TFSI)_2$, respectively. The value of b_n (n = 1−4) is the fitted *b* value for redox peak *n* in the CV curves.

$$\text{Cathode: EMD } (MnO_2) + H^+ + e^- \leftrightarrow MnOOH$$

$$1/6ZnSO_4 + OH^- + 1/2Zn^{2+} + n/6H_2O \leftrightarrow 1/6ZnSO_4[Zn(OH)_2]_3 \cdot nH_2O$$

$$\text{Anode: } 1/2Zn \leftrightarrow 1/2Zn^{2+} + e^-$$

XRD peaks for MnOOH in the discharged EMD electrodes were submerged in the strong peaks from $ZnSO_4[Zn(OH)_2]_3 \cdot nH_2O$ (Figure S6). When charged back to 1.8 V, the XRD pattern shows that $Zn_4SO_4(OH)_6 \cdot nH_2O$ reversibly decomposed, and the EMD electrode changed back to its original crystal phase in Figure 3b.

The discharge and charge products on EMD electrodes in 3 M $Zn(TFSI)_2$ electrolyte were investigated after DI water rinsing in Figure 3c and 3d. Complete water rinsing for EMD electrodes effectively avoids the interference of XRD peaks from $Zn(TFSI)_2$-based discharge products as shown in Figure S7. After discharging to 1 V, the original EMD peak disappeared along with the formation of MnOOH as shown in Figure 3c. The formation of the discharge compound MnOOH was further confirmed in the following cycles in Figure 3d. The MnOOH phase and the accompanied compound $Zn(TFSI)_2[Zn(OH)_2]_3 \cdot mH_2O$ reversibly disappeared, and the EMD electrode recovered back to the original EMD phase (Figure 3c) after charging back to 1.8 V. Zinc hydroxyl compounds such as $ZnSO_4[Zn(OH)_2]_3 \cdot nH_2O$ have been widely investigated as precursors for ZnO synthesis in the literature,[31−33] in which the $ZnSO_4$ can be replaced by $ZnCl_2$ or $ZnCO_3$ salts, etc.[34,35] The discharge product $Zn(TFSI)_2[Zn(OH)_2]_3 \cdot mH_2O$ is considered to be an analogy compound of $ZnSO_4[Zn(OH)_2]_3 \cdot nH_2O$,[19] which is formed through the proposed reactions in an electrochemical process:

$$\text{Cathode: EMD}(MnO_2) + H^+ + e^- \leftrightarrow MnOOH$$

$$1/6Zn(TFSI)_2 + OH^- + 1/2Zn^{2+} + m/6H_2O \leftrightarrow 1/6Zn(TFSI)_2[Zn(OH)_2]_3 \cdot mH_2O$$

$$\text{Anode: } 1/2Zn \leftrightarrow 1/2Zn^{2+} + e^-$$

The XRD results for EMD electrodes indicate the same reversible reaction between EMD and H^+ ion forming MnOOH in both $ZnSO_4$- and $Zn(TFSI)_2$-based aqueous electrolytes. In addition, the preaddition of Mn^{2+} ions in aqueous electrolytes does not affect the structural evolution of EMD cathodes during charge and discharge, indicating the same phase change redox reactions in EMD cathodes with and without Mn^{2+} addition as discussed in Figure S8 and Figure S9. Interestingly, small XRD peaks at 36.56° and 59.6° from the original EMD phase were still observed besides the formation of MnOOH at the discharged state in $Zn(TFSI)_2$-based electrolyte as shown in Figure 3d. This could be from the EMD not participating in redox reactions or from special redox reactions in EMD material that is free of crystal phase change during the charge−discharge process (to be discussed later).

The electrochemical reaction kinetics parameters were symmetrically investigated to further understand the redox reactions in EMD cathodes in Figure 4. The various sweep rates of CV curves of EMD cathodes in 1 M $ZnSO_4$, 3 M $Zn(TFSI)_2$, and 3 M $Zn(TFSI)_2$ + 0.1 M $Mn(TFSI)_2$ electrolytes were presented in Figure 4a, 4c, and 4e, respectively, and in Figure S10. It was noted that metal oxide electrodes with a conversion reaction usually exhibit a difference in the first and second charge−discharge curves due to modification of thermodynamic energy of the electrode after the first discharge (Figure S1),[36] and the reaction kinetics were mainly determined after the first cycle. Therefore, the second cycle charge−discharge curves and CV scanning curves were employed to analyze the reaction kinetics in EMD in this work. Significantly different CV curves for EMD electrodes in different electrolytes suggest a different reaction pathway and mechanisms. In addition, a new oxidation CV peak at 1.4 V

DOI: 10.1021/acsami.9b09252
ACS Appl. Mater. Interfaces XXXX, XXX, XXX−XXX

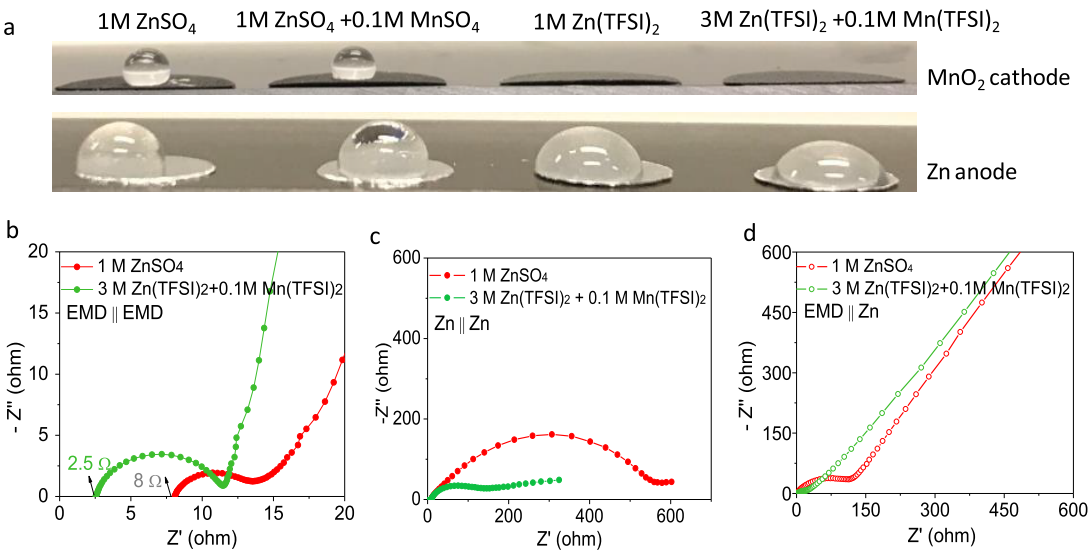

Figure 5. (a) Wettability of different electrolytes on fresh EMD cathode and Zn anode. The electrochemical impedance of spectra for (b) fresh symmetrical EMD||EMD, (c) fresh Zn||Zn cell, and (d) EMD||Zn cell discharged to 1 V in the first cycle.

(peak 3 in Figure 4c and 4e) appeared in $Zn(TFSI)_2$-based electrolytes, which is consistent with the observation in the electrolyte of 1 M $Zn(TFSI)_2$ in Figure 2a.

The current (i) of redox peak of CV scanning exhibits a correlation with scanning rate (v) according to the equation of $i = av^b$,[37,38] where a and b normally vary in a range of 0.5−1, depending on the charge storage mechanisms and reaction kinetics of EMD cathodes. For a redox reaction that is limited by solid-state diffusion of charge storage ions, the b value is 0.5, whereas for a redox reaction that is a nondiffusion-controlled electrochemical capacitive process, the b value is 1.[37] The correlation between log (i) and log (v) for redox peaks in different electrolytes is presented in a sweep rate ranging from 0.1 mV s^{-1} to 10 mV s^{-1}, respectively, in Figure 4b, 4d, and 4f. The slopes of log (i)−log (v) dependence curves for peak 1 and peak 3 in 1 M $ZnSO_4$ electrolyte were shown in Figure 4b. The curve for peak 2 is not plotted due to the inconspicuous peaks under higher sweep rates (Figure S10). A two-region feature for slopes is obviously observed. In region 1 (lower scan rate: <0.2 mV s^{-1}), the pair of redox peaks 1 and 3 shows a higher b value close to 1, indicating the redox reaction is diffusion-free. In region 2 (faster scan rate: >0.4 mV s^{-1}), the slopes changed significantly with a reduced b value of 0.5 for peak 1 and peak 3, respectively. The b value of 0.5 indicates diffusion constraints for redox reactions in EMD electrode in 1 M $ZnSO_4$ electrolyte in such a scan range. The diffusion-controlled reaction is normally accompanied by a crystal phase change of electrode material during charge and discharge.[37] In the faster scanning region 2, the effective capacity in EMD electrode is contributed by the diffusion-controlled H^+ reaction with EMD, forming a new crystal phase of MnOOH as discussed in Figure 3. The main redox reactions with crystal phase change in EMD material make the cycling stability of EMD challenging in $ZnSO_4$-based electrolyte, which could account for the faster capacity degradation as discussed in Figure 2c. In contrast, the two-region feature for the EMD cathode in $Zn(TFSI)_2$-based electrolytes became not obvious as shown in Figure 4d and 4f. The main redox peaks (peak 1 and peak 4) present higher b values than those in $ZnSO_4$ electrolyte in a wide scan range (0.1−10 mV s^{-1}), indicating the increase of diffusion-free redox reactions in EMD with $Zn(TFSI)_2$-based electrolytes. The addition of 0.1 M $Mn(TFSI)_2$ further enhanced the nondiffusion redox reactions with increased b values (Figure S10c and Figure 4f).

The b values in a range of 0.5−1 for the redox peaks in EMD suggest a mixed charge storage mechanism with both diffusion-controlled and diffusion-free redox reactions. The part of diffusion-limited reactions in EMD—conversion reaction between EMD and H^+ forming MnOOH—is similar in both $ZnSO_4$-based and $Zn(TFSI)_2$-based electrolytes as discussed in Figure 3. The part of diffusion-free capacity could be from "pseudocapacitance"-like reactions in EMD electrode, such as diffusion-free Zn^{2+} ion storage in the hierarchical nano-composite EMD material.[19] The redox peak in CV curves for EMD in Figure 2a and Figure 4a, 4c, and 4e should be contributed by both diffusion-controlled conversion reaction with H^+ and "pseudocapacitance" storage in EMD, for which the electrolyte media and scanning rate are important to determine the contribution for each redox peak in EMD electrodes. The $Zn(TFSI)_2$-based electrolyte is beneficial to the diffusion-free "pseudocapacitance" redox reactions that are free of crystal phase change in EMD and thus favors the structural stability of EMD and enables better cycling stability as discussed in Figure 2. Such diffusion-free reactions could account for the still observed EMD peaks after discharge in Figure 3d in the $Zn(TFSI)_2$-based electrolyte. This is consistent with our previous report on the electrolyte-dependent joint charge storage reactions in a layered δ-MnO_2 cathode,[19] suggesting the mixed charge storage in MnO_2 is mainly related to the used electrolyte rather than a special crystal phase of MnO_2.

In addition, the electrode surface properties of the EMD cathode and Zn anode were further investigated in Figure 5. The electrolyte wettability on the EMD cathode and Zn anode is shown in Figure 5a. It was found that the $ZnSO_4$-based electrolyte exhibits poor wettability on either a cathode or anode, whereas the $Zn(TFSI)_2$-based electrolyte penetrates into the EMD cathode immediately, showing excellent wettability; the electrolyte wettability on Zn metal is also improved compared with $ZnSO_4$-based electrolyte. The electrochemical impedance (EIS) measurements for EMD||EMD and Zn||Zn cells show a lower system resistance

DOI: 10.1021/acsami.9b09252
ACS Appl. Mater. Interfaces XXXX, XXX, XXX−XXX

(R_s) and lower charge transfer resistance on the fresh Zn metal side in 3 M $Zn(TFSI)_2$ + 0.1 $Mn(TFSI)_2$ electrolyte compared with those in 1 M $ZnSO_4$ electrolyte (Figure 5b and 5c). The EMD||Zn full cell presents 5 times lower overall charge transfer resistance after the first discharge in 3 M $Zn(TFSI)_2$ + 0.1 $Mn(TFSI)_2$ electrolyte (Figure 5d). The reduced electrochemical impedance in $Zn(TFIS)_2$-based electrolyte could be associated with the good electrolyte wettability on the EMD cathode and anode, which further enhances the redox reactions in EMD cathode and improves the cycling stability of Zn-EMD batteries.

■ CONCLUSION

We demonstrate low-cost and commercially available EMD material as a promising cathode material for the application of long-life and high-rate mild aqueous rechargeable Zn-MnO_2 batteries. The correlation between the effective redox reaction mechanisms and the electrochemical performance of the EMD cathode was identified. The EMD cathode exhibits a controllable mixed diffusion-controlled conversion reaction and diffusion-free "pseudocapacitance"-like charge storage mechanism according to the employed electrolyte. Zn-$(TFSI)_2$-based electrolyte favors more diffusion-free redox reactions in EMD and good electrolyte wettability, thus improving the structural stability of EMD and cycling stability. Highly reversible reactions for Zn-EMD batteries were demonstrated with excellent cycling stability over 5000 cycles and a capacity retention of 94.6% in optimal $Zn(TFSI)_2$ electrolyte. This study provides useful guidance to develop high performance mild aqueous Zn-MnO_2 batteries through a rational control of the reaction mechanisms and electrode surface properties in different electrolytes.

■ ASSOCIATED CONTENT

Supporting Information

The Supporting Information is available free of charge on the ACS Publications website at DOI: 10.1021/acsami.9b09252.

Charge−discharge curves, ICP measurement of electrolytes, CV scanning, and XRD measurement of EMD electrodes (PDF)

■ AUTHOR INFORMATION

Corresponding Author

*E-mail: panhuilinpy@gmail.com.

ORCID

Huilin Pan: 0000-0001-7991-1015

Present Address

†The Department of Chemistry at Zhejiang University, Hangzhou, Zhejiang, 310028, China.

Notes

The authors declare no competing financial interest.

■ ACKNOWLEDGMENTS

This work was supported by the U.S. Department of Energy (DOE) Office of Electricity Delivery and Energy Reliability (Contract No. 57558) and the Pacific Northwest National Laboratory, which is a multiprogram laboratory operated by Battelle Memorial Institute for the DOE under Contract DE-AC05-76RL01830.

■ REFERENCES

(1) Marsal, P. A.; Karl, K.; Urry, L. F. Dry Cell. 1960, US Patent 2,960,558.

(2) Falk, S. U.; Salkind, A. J. *Alkaline Storage Batteries*; Book, 1969. EDB-84-107852.

(3) Pan, H.; Shao, Y.; Yan, P.; Cheng, Y.; Han, K. S.; Nie, Z.; Wang, C.; Yang, J.; Li, X.; Bhattacharya, P.; Mueller, K. T.; Liu, J. Reversible Aqueous Zinc/Manganese Oxide Energy Storage from Conversion Reactions. *Nat. Energy* **2016**, *1*, 16039.

(4) Zhang, N.; Cheng, F.; Liu, J.; Wang, L.; Long, X.; Liu, X.; Li, F.; Chen, J. Rechargeable Aqueous Zinc-Manganese Dioxide Batteries with High Energy and Power Densities. *Nat. Commun.* **2017**, *8*, 405.

(5) Huang, J.; Wang, Z.; Hou, M.; Dong, X.; Liu, Y.; Wang, Y.; Xia, Y. Polyaniline-Intercalated Manganese Dioxide Nanolayers as a High-Performance Cathode Material for an Aqueous Zinc-Ion Battery. *Nat. Commun.* **2018**, *9*, 2906.

(6) Yadav, G. G.; Gallaway, J. W.; Turney, D. E.; Nyce, M.; Huang, J.; Wei, X.; Banerjee, S. Regenerable Cu-Intercalated MnO_2 Layered Cathode for Highly Cyclable Energy Dense Batteries. *Nat. Commun.* **2017**, *8*, 14424.

(7) Amano, Y.; Ogawa, H.; Umeo, Y.; Ohira, T.; Murakami, K., Rechargeable Alkaline Manganese Cell. 1970, US Patent US3530496A.

(8) Mondoloni, C.; Laborde, M.; Rioux, J.; Andoni, E.; Lévy-Clément, C. Rechargeable Alkaline Manganese Dioxide Batteries: I. In Situ X-Ray Diffraction Investigation of the (EMD-Type) Insertion System. *J. Electrochem. Soc.* **1992**, *139*, 954−959.

(9) Im, D.; Manthiram, A.; Coffey, B. Manganese(III) Chemistry in KOH Solutions in the Presence of Bi- or Ba-Containing Compounds and Its Implications on the Rechargeability of γ MnO_2 in Alkaline Cells. *J. Electrochem. Soc.* **2003**, *150*, A1651−A1659.

(10) Huang, J.; Yadav, G. G.; Gallaway, J. W.; Wei, X.; Nyce, M.; Banerjee, S. A Calcium Hydroxide Interlayer as a Selective Separator for Rechargeable Alkaline Zn/MnO_2 Batteries. *Electrochem. Commun.* **2017**, *81*, 136−140.

(11) González, M.; Trócoli, R.; Pavlovic, I.; Barriga, C.; La Mantia, F. Layered Double Hydroxides as a Suitable Substrate to Improve the Efficiency of Zn Anode in Neutral pH Zn-ion Batteries. *Electrochem. Commun.* **2016**, *68*, 1−4.

(12) Sun, K. E.; Hoang, T. K.; Doan, T. N. L.; Yu, Y.; Zhu, X.; Tian, Y.; Chen, P. Suppression of Dendrite Formation and Corrosion on Zinc Anode of Secondary Aqueous Batteries. *ACS Appl. Mater. Interfaces* **2017**, *9*, 9681−9687.

(13) Wang, F.; Borodin, O.; Gao, T.; Fan, X.; Sun, W.; Han, F.; Faraone, A.; Dura, J. A.; Xu, K.; Wang, C. Highly Reversible Zinc Metal Anode for Aqueous Batteries. *Nat. Mater.* **2018**, *17*, 543.

(14) Xu, C.; Li, B.; Du, H.; Kang, F. Energetic Zinc Ion Chemistry: The Rechargeable Zinc Ion Battery. *Angew. Chem., Int. Ed.* **2012**, *51*, 933−935.

(15) Lee, B.; Lee, H. R.; Kim, H.; Chung, K. Y.; Cho, B. W.; Oh, S. H. Elucidating the Intercalation Mechanism of Zinc Ions into α-MnO_2 for Rechargeable Zinc Batteries. *Chem. Commun.* **2015**, *51*, 9265−9268.

(16) Alfaruqi, M. H.; Mathew, V.; Gim, J.; Kim, S.; Song, J.; Baboo, J. P.; Choi, S. H.; Kim, J. Electrochemically Induced Structural Transformation in a γ-MnO_2 Cathode of a High Capacity Zinc-Ion Battery System. *Chem. Mater.* **2015**, *27*, 3609−3620.

(17) Alfaruqi, M. H.; Gim, J.; Kim, S.; Song, J.; Pham, D. T.; Jo, J.; Xiu, Z.; Mathew, V.; Kim, J. A Layered δ-MnO_2 Nanoflake Cathode with High Zinc-Storage Capacities for Eco-friendly Battery Applications. *Electrochem. Commun.* **2015**, *60*, 121−125.

(18) Sun, W.; Wang, F.; Hou, S.; Yang, C.; Fan, X.; Ma, Z.; Gao, T.; Han, F.; Hu, R.; Zhu, M.; Wang, C. Zn/MnO2 Battery Chemistry with H^+ and Zn^{2+} Coinsertion. *J. Am. Chem. Soc.* **2017**, *139*, 9775−9778.

(19) Jin, Y.; Zou, L.; Liu, L. L.; Engelhard, M. H.; Patel, R. L.; Nie, Z. N.; Han, K. S.; Shao, Y. S.; Wang, C.; Zhu, J.; Pan, H.; Liu, J. Joint Charge Storage for High-Rate Aqueous Zinc-Manganese Dioxide Batteries. *Adv. Mater.* **2019**, *31*, 1900567.

DOI: 10.1021/acsami.9b09252
ACS Appl. Mater. Interfaces XXXX, XXX, XXX−XXX

(20) Biswal, A.; Chandra Tripathy, B.; Sanjay, K.; Subbaiah, T.; Minakshi, M. Electrolytic Manganese Dioxide (EMD): a Perspective on Worldwide Production, Reserves and its Role in Electrochemistry. *RSC Adv.* **2015**, *5*, 58255−58283.

(21) Biswal, A.; Sanjay, K.; Ghosh, M.; Subbaiah, T.; Mishra, B. Preparation and Characterization of EMD from Manganese Cake—A Byproduct of Manganese Nodule Processing. *Hydrometallurgy* **2011**, *110*, 44−49.

(22) Simon, D.; Morton, R.; Gislason, J. A Close Look at Electrolytic Manganese Dioxide (EMD) and the γ-MnO_2 & ε-MnO_2 Phases Using Rietveld Modeling. *Adv. X-ray Anal* **2004**, *47*, 267−280.

(23) Ghaemi, M.; Binder, L. Effects of Direct and Pulse Current on Electrodeposition of Manganese Dioxide. *J. Power Sources* **2002**, *111*, 248−254.

(24) Kim, S. H.; Oh, S. M. Degradation Mechanism of Layered MnO_2 Cathodes in $Zn/ZnSO_4/MnO_2$ Rechargeable Cells. *J. Power Sources* **1998**, *72*, 150−158.

(25) Han, S.-D.; Kim, S.; Li, D.; Petkov, V.; Yoo, H. D.; Phillips, P. J.; Wang, H.; Jae Jin Kim, J. J.; More, K. L.; Key, B.; Klie, R. F.; Cabana, J.; Stamenkovic, V. R.; Fister, T. T.; Markovic, N. M.; Burrell, A. K.; Tepavcevic, S.; Vaughey, J. T. Mechanism of Zn Insertion into Nanostructured δ-MnO_2: A Nonaqueous Rechargeable Zn Metal Battery. *Chem. Mater.* **2017**, *29*, 4874−4884.

(26) Oaks, H. H.; Bradt, W. The Electrodeposition of Manganese from Aqueous Solutions I. Chloride Electrolytes. *Trans. Electrochem. Soc.* **1936**, *69*, 567−584.

(27) Shelton, S. M.; Royer, M. B. Effect of Solution Concentration in Electrodeposition of Manganese. *Trans. Electrochem. Soc.* **1938**, *74*, 447−459.

(28) Kozawa, A.; Vosburgh, W. The Relation of the Conditions of Electrodeposition of Manganese Dioxide to the Discharge Characteristics. *J. Electrochem. Soc.* **1958**, *105*, 59−63.

(29) Nakayama, M.; Shamoto, M.; Kamimura, A. Surfactant-Induced Electrodeposition of Layered Manganese Oxide with Large Interlayer Space for Catalytic Oxidation of Phenol. *Chem. Mater.* **2010**, *22*, 5887−5894.

(30) Suo, L.; Borodin, O.; Gao, T.; Olguin, M.; Ho, J.; Fan, X.; Luo, C.; Wang, C.; Xu, K. Water-in-Salt Electrolyte Enables High-Voltage Aqueous Lithium-Ion Chemistries. *Science* **2015**, *350*, 938−943.

(31) Moezzi, A.; Cortie, M. B.; McDonagh, A. M. Zinc Hydroxide Sulphate and its Transformation to Crystalline Zinc Oxide. *Dalton Trans.* **2013**, *42*, 14432−14437.

(32) Darezereshki, E.; Alizadeh, M.; Bakhtiari, F.; Schaffie, M.; Ranjbar, M. A Novel Thermal Decomposition Method for the Synthesis of ZnO Nanoparticles from Low Concentration $ZnSO_4$ Solutions. *Appl. Clay Sci.* **2011**, *54*, 107−111.

(33) Dziedzic, R. M.; Gillian-Daniel, A. L.; Petersen, G. M.; Martínez-Hernández, K. J. Microwave Synthesis of Zinc Hydroxy Sulfate Nanoplates and Zinc Oxide Nanorods in the Classroom. *J. Chem. Educ.* **2014**, *91*, 1710−1714.

(34) Odnevall, I.; Leygraf, C. The Formation of $Zn_4Cl_2(OH)_4SO_4 \cdot 5H_2O$ in an Urban and an Industrial Atmosphere. *Corros. Sci.* **1994**, *36*, 1551−1559.

(35) Li, Z.; Shen, X.; Feng, X.; Wang, P.; Wu, Z. Non-isothermal Kinetics Studies on the Thermal Decomposition of Zinc Hydroxide Carbonate. *Thermochim. Acta* **2005**, *438*, 102−106.

(36) Zhong, K.; Zhang, B.; Luo, S.; Wen, W.; Li, H.; Huang, X.; Chen, L. Investigation on Porous MnO Microsphere Anode for Lithium Ion Batteries. *J. Power Sources* **2011**, *196*, 6802−6808.

(37) Augustyn, V.; Come, J.; Lowe, M. A.; Kim, J. W.; Taberna, P.-L.; Tolbert, S. H.; Abruña, H. D.; Simon, P.; Dunn, B. High-Rate Electrochemical Energy Storage Through Li^+ Intercalation Pseudocapacitance. *Nat. Mater.* **2013**, *12*, 518.

(38) Liu, T. C.; Pell, W.; Conway, B.; Roberson, S. Behavior of Molybdenum Nitrides as Materials for Electrochemical Capacitors Comparison with Ruthenium Oxide. *J. Electrochem. Soc.* **1998**, *145*, 1882−1888.

DOI: 10.1021/acsami.9b09252
ACS Appl. Mater. Interfaces XXXX, XXX, XXX−XXX